Visual-Vestibular Feedback for Enhanced Situational Awareness in Teleoperation of UAVs

P. Robuffo Giordano, H. Deusch, J. Lächele*, and H. H. Bülthoff†

This paper presents a novel concept for improving the situational awareness of a ground operator in remote control of a Unmanned Arial Vehicle (UAV). To this end, we propose to integrate vestibular feedback with the usual visual feedback obtained from a UAV onboard camera. We use our motion platform, the CyberMotion simulator, so as to reproduce online the desired motion cues. We test this architecture by flying a small-scale quadcopter and run a detailed performance evaluation on 12 test subjects. We then discuss the results in terms of possible benefits for facilitating the remote control task.

Introduction

Use of Unmanned Aerial Vehicles (UAVs) to remotely perform tasks is an active research field. The possible applications range from dealing with hazardous environments, to search and rescue operations, and to surveillance and inspection of sites. An overview of the state of the art can be found in (Ref. 1). Depending on the particular application, different degrees of autonomy can be assigned to the controlled UAVs. The division of roles between remote agents and human operators can be classified as *direct control*, *supervisory control*, and *shared control*, see also the discussion in (Ref. 2). In any case, a successful synergy between humans and remote vehicles is inherently dependent on the quality of situational awareness that an operator can obtain from the remote information he receives.

Ideally, a perfect remote presence, or *telepresence*, should enable the operator to perceive the remote environment as if sensed directly. Such a system should then reproduce the full multisensory flow of information that humans experience through their senses: vision, haptics, hearing, vestibular (self-motion) information, and even smell and taste. In practice, the operator's situational awareness is often degraded by the limited quality and quantity of information that can be provided through ad-hoc Human-Machine Interfaces (HMIs) (Ref. 3). Indeed, most HMI setups only rely on visual feedback from UAV onboard cameras, possibly augmented with superimposed artifacts describing additional information. However, if the visual channel gets too overloaded, the operator can likely miss important information and become quickly fatigued or distracted.

*P. Robuffo Giordano, H. Deusch, and J. Lächele are with the Max Planck Institute for Biological Cybernetics, Spemannstraße 38, 72076 Tübingen, Germany.

†H. H. Bülthoff is with the Max Planck Institute for Biological Cybernetics, Spemannstraße 38, 72076 Tübingen, Germany, and with the Department of Brain and Cognitive Engineering, Korea University, Anam-dong, Seongbuk-gu, Seoul, 136-713 Korea.

Additionally, UAVs are vulnerable to atmospheric conditions, such as wind gusts, especially near structures or obstacles, or in sensitive phases such as taking off and landing (Ref. 4). In a remote control scenario, poor operator's situational awareness can lead to wrong reactions and, in the worst case, complete loss of the vehicle. Consider the well-known case of the *Predator*, a large UAV used by the United States Air Forces for reconnaissance missions in Iraq and Afghanistan (Ref. 5). It has been reported that, during the Afghan campaign, the US Air Force lost several of them in action mainly because of foul weather, particularly icy conditions (Ref. 6). Of course, in domains where safety is an issue, such as flying in cluttered environments or at low altitudes over populated areas, or performing sensitive missions, limitations due to poor situational awareness can pose a severe restriction in the use of remote-controlled UAVs.

Most of the existing HMIs for remote vehicles focus on visual and/or auditory or haptic feedback, but pay little or no attention to vestibular feedback. Here, by vestibular feedback, we refer to the perception of self linear/angular motion through the integration of the inertial information provided by the semicircular canals and otoliths in the human's ears. The vestibular system is an important sensory input in self stabilization and quick balance tasks, and, besides vision, provides pilots with important information on their motion status (Refs. 7–12). Within tasks involving flying vehicles, a pilot could 'feel' the effect of unexpected atmospheric disturbances as a sudden change of his/her motion, and quickly react to stabilize the vehicle. This, of course, would be particularly relevant for small and medium size UAVs for which the ratio between aerodynamic loads and vehicle mass grows as the inverse of size (mass).

In this respect, the aim of this paper is to investigate, in a UAV remote control task, the possible benefits of integrating vestibular feedback with the visual feedback obtained from a UAV onboard camera. As a means to provide vestibular cues, we exploit a motion simulator platform carrying the human operator in control of the UAV so as to re-

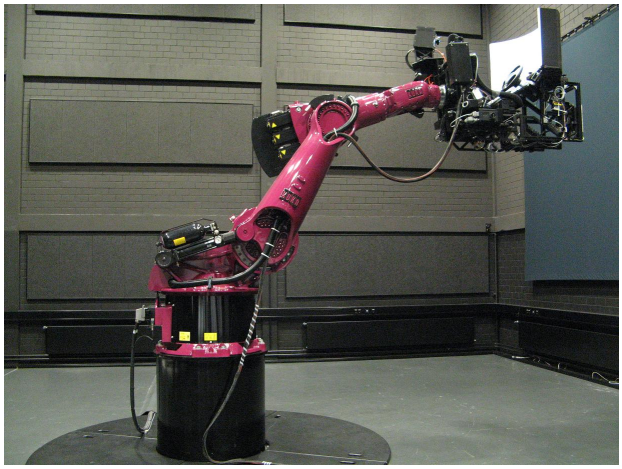

Fig. 1: A snapshot of the CyberMotion Simulator

produce online the desired motion feedback. A similar concept was also explored in (Refs. 13, 14) for remotely controlling a ground vehicle, and in a recent paper (Ref. 15) for remote UAV operation. This work, however, only focuses on the technological and system architecture needed for realizing the proposed concept of UAV teleoperation with visual/vestibular feedback, and postpones any human evaluation to later studies. Therefore, to the best of our knowledge, our paper is the first to systematically investigate the possible benefits of vestibular feedback in terms of human piloting performance.

The rest of the paper is organized as follows. We first describe our experimental setup, i.e.,

1. a 6-DOFs anthropomorphic robot manipulator used as a motion platform, the CyberMotion motion simulator;
2. a small-scale quadcopter used as remotely controlled UAV;
3. a large tracking hall equipped with the VICON motion capture system (Ref. 16) used for tracking online the UAV pose.

We then illustrate the experimental procedure chosen to test the effects of combining visual and vestibular feedbacks for remote UAV operation, and report and discuss the experimental results. Finally, in the last Section we draw the conclusions and discuss open points and future directions.

Description of the experimental setup

The CyberMotion simulator

The CyberMotion simulator consists of a standard 6-DOFs anthropomorphic robot arm, see Fig. 1. It is based on the commercial KUKA Robocoaster (Ref. 17) (a modified KR-500 industrial robot with a 500 [Kg] payload), which was originally designed for use in amusement parks. A cabin

Fig. 2: The UAV used in our experiments instrumented with reflective markers to be tracked by our Vicon system

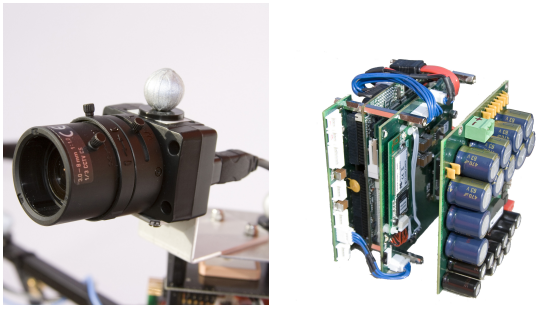

(a) (b)

Fig. 3: The PTGrey Firefly camera (a), the Quadcopter Flight Computer (QFC) and the transformer board with a size of $10.0 \times 7.2 \times 7.5$ cm (b)

with an onboard projection system is rigidly attached to the robot end-effector, and can be equipped with different kinds of input devices. Several details on the robot mechanical and software characteristics can be found in (Ref. 18). A number of experiments on pilot modeling in closed-loop tasks and transfer of training in flying simplified models of an helicopter have already been designed and run on the CyberMotion simulator, see (Refs. 19–21). More recently, we also developed a control framework for fully exploiting the 6-DOFs robot motion capabilities through a suitable online inverse kinematics and motion cueing algorithm tailored to the specific robot workspace (Refs. 22, 23). This framework, whose conceptual scheme is depicted in Fig. 4, was exploited in our experiments in order to provide the operator with the desired motion cues.

The UAV

As UAV, we used a small-scale commercial quadcopter, the *MikroKopter L4-ME* model made by the company HiSystems GmbH (Ref. 24), see Fig. 2 for a snapshot. This small-scale quadcopter is meant to represent the qualitative behavior of a generic rotorcraft vehicle, e.g., possibility to hover or to perform sideways movements.

The standard quadcopter onboard electronics and sen-

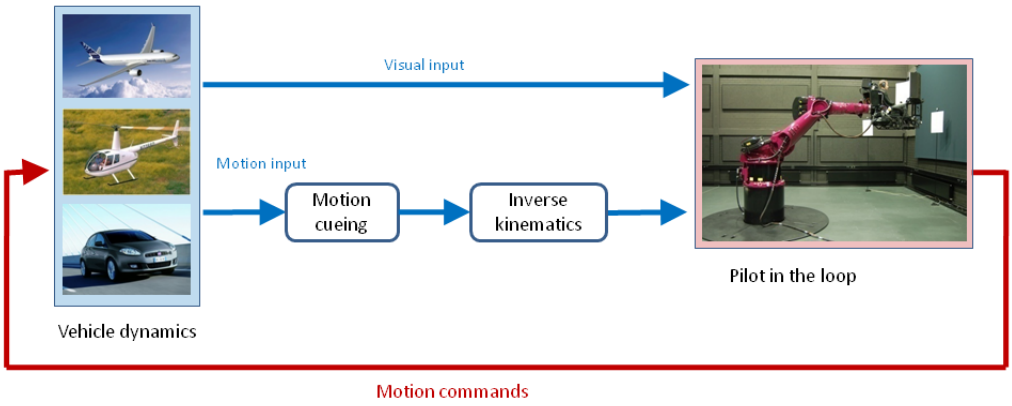

Fig. 4: A block-scheme representation of the typical motion simulation loop

sors allow for semi-autonomous flight control. In particular, a built-in *Flight Controller* processes data from 3 MEMS gyroscopes, 3D accelerometers and a pressure sensor, and actuates the 4 quadcopter propellers. These consist of four 25 cm rotors, each attached to one *Roxxy MK2832/35* motor. The distance between the centers of two opposing rotors is 48 cm. For outdoor flight a LiPo accumulator is used as energy source, whilst for indoor experiments the quadcopter was powered by a ground based AC adapter. The *Flight Controller* executes a low-level control loop in charge of realizing 4 'high-level' motion input commands. With reference to Fig. 5, let $E : \{X_E, Y_E, Z_E\}$ be an earth fixed reference frame, and $B : \{X_B, Y_B, Z_B\}$ be a body-fixed frame[1]. The 4 quadcopter commands are then: vertical thrust τ (along Z_B), roll angle ϕ (rotation around X_B), pitch angle θ (rotation around Y_B), and yaw rate $\dot{\psi}$ (angular velocity around Z_B).

Besides these hardware components, we equipped the quadcopter with a digital camera (Fig. 3(a)), an additional embedded PC board (the Quadcopter Flight Computer (QFC), Fig. 3(b)), and 5 reflective markers used for external optical tracking (Fig. 2). The camera faces the forward direction (X_B axis in Fig. 5), and captures 24 Bit RGB pictures with a resolution of 640×480 pixels up to 30 frames per second. These pictures are transferred to the QFC via a USB connection. The QFC features an Intel Atom 1.6 GHz processor, 2 GB of DDR-RAM, a 128 GB solid state drive and a 144 Mbs Wireless LAN module.

For simulation and testing purposes, we also developed a mathematical model of the quadcopter based on standard rigid body dynamics as described in (Ref. 25). We neglected aerodynamic forces and only considered the effects of gravity and propeller thrusts. The action of the low-level *Flight Controller* was also included in the simulation, thus obtaining the same input interface of the real quadcopter,

[1]Note that the in both frames the Z-axes point downwards according to the standard aeronautical convention.

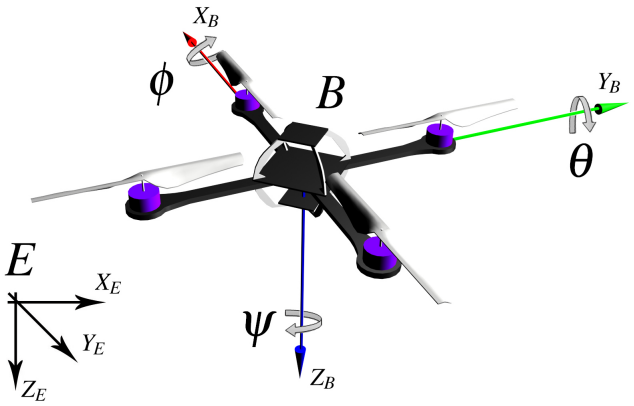

Fig. 5: Frame system with body fixed frame B and earth fixed frame E

i.e., the 4 commands $(\tau, \phi, \theta, \dot{\psi})$ described before. This simulation model was used in place of the real quadcopter during half of the experiments described in the subsequent Sections.

Tracking hall

The experiments were conducted in a tracking hall consisting of a large, fully tracked, freewalking space of 12.8 by 11.7 m in size (see Fig. 8(a)). An optical system (16 Vicon MX13 cameras, see Fig. 8(b)) tracks online the reflective markers attached to the quadcopter and reconstructs its 6-DOFs pose at a frequency of 120 Hz. We used this tracking facility for obtaining accurate ground-truth data of the quadcopter motion.

System architecture

Figure 6 illustrates the main components and communication paths present in our experimental setup. Starting from

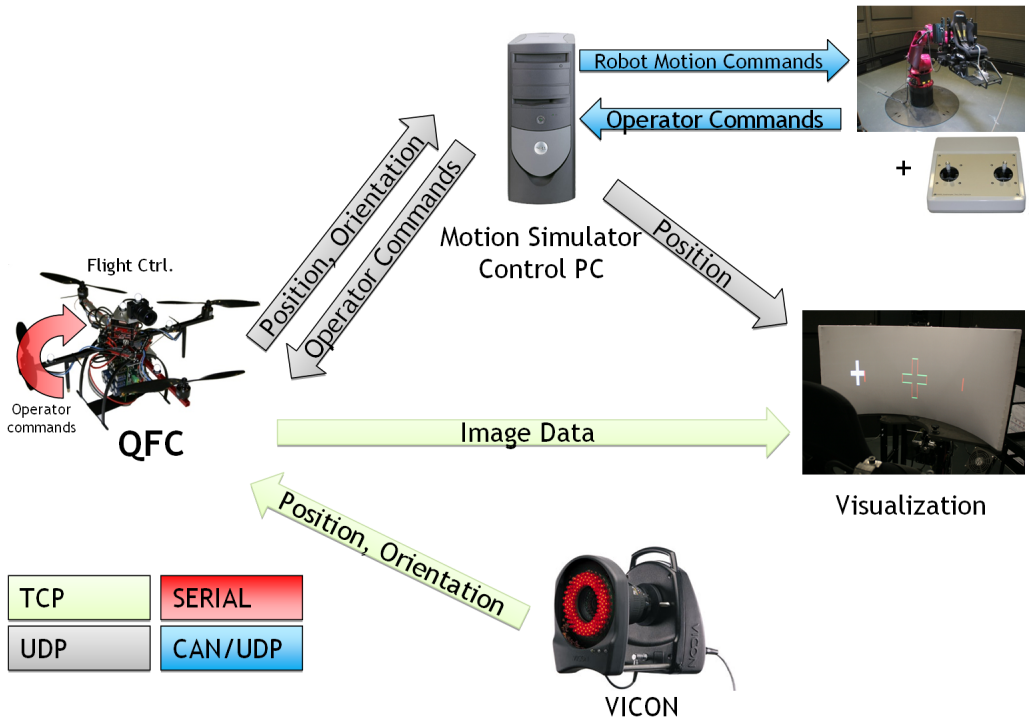

Fig. 6: Network diagram of the experiment setup

the left, the QFC receives through a wireless link the 6-DOFs quadcopter pose from the Vicon system. This is both used internally for implementing a collision avoidance algorithm (explained in the next Section), and forwarded via the wireless link to the motion simulator control PC that uses this data for determining the motion feedback provided to the operator. The QFC is also connected to a Visualization PC to which it sends the onboard camera images at a rate between 20 and 25 fps. These are then displayed to the operator on the screen mounted on the motion simulator cabin.

The motion simulator control PC reads the control inputs of the operator (Fig. 9 shows the used input device) which are then sent back to the QFC for their actual realization, and executes the control software that actuates the motion simulator for providing the desired vestibular cues. Furthermore, it also forwards to the Visualization PC the current quadcopter position. This is used by the Visualization PC for displaying some artificial visual aids during the experiment (see next Section).

Methods

Control task

As control task, we chose a planar hovering task in which the test subjects had to regulate the quadcopter position from a starting location $P_0 = (0, 0, -2.5)$ m to a desired goal location $P_1 = (2.5, -2.5, -2.5)$ m in the world frame E (Fig. 11). The task was considered completed when they could stay within a box B centered at P_1 with edges of 0.03 m for 3 s. In order to simplify the control task, the available quadcopter inputs $(\tau, \phi, \theta, \dot{\psi})$ were reduced to the pair (ϕ, θ) roll/pitch commands by implementing on the QFC a custom-made height and yaw controller. The yaw was constantly held to 0 deg by means of a P-controller acting on the $\dot{\psi}$ input (yaw rate), while the height (in the absolute frame) was regulated to 2.5 m by a PD-controller acting on the τ input (vertical thrust). Therefore, the test subjects could only control the planar forward and lateral accelerations of the quadcopter by acting on the right stick of their input device, see Fig. 9. Here, the two stick commands $s_\phi \in [-1, 1]$ and $s_\theta \in [-1, 1]$ were linearly mapped to the roll $\phi \in [-15, 15]$ deg and pitch $\theta \in [-15, 15]$ deg inputs of the quadcopter. In addition to this, we also implemented a simple collision avoidance algorithm that uses the Vicon readings for monitoring the distance to the tracking hall walls, and overrides any user command when trespassing a predetermined threshold.

Figures 7 illustrate the visual feedback given to the operator during each trial. A white vertical cross on the facing wall in the tracking hall acts as external visual landmark to be compared with a synthetic wireframe cross superimposed on the camera images. This wireframe cross is chosen so that, when at P_1, it perfectly coincides with the contour of the white cross on the wall (Fig. 7(b)). To further help in judging the forward distance to the target (the depth), another visual cue was added. Two dots, one on the right side and one on the left side of the camera image, were

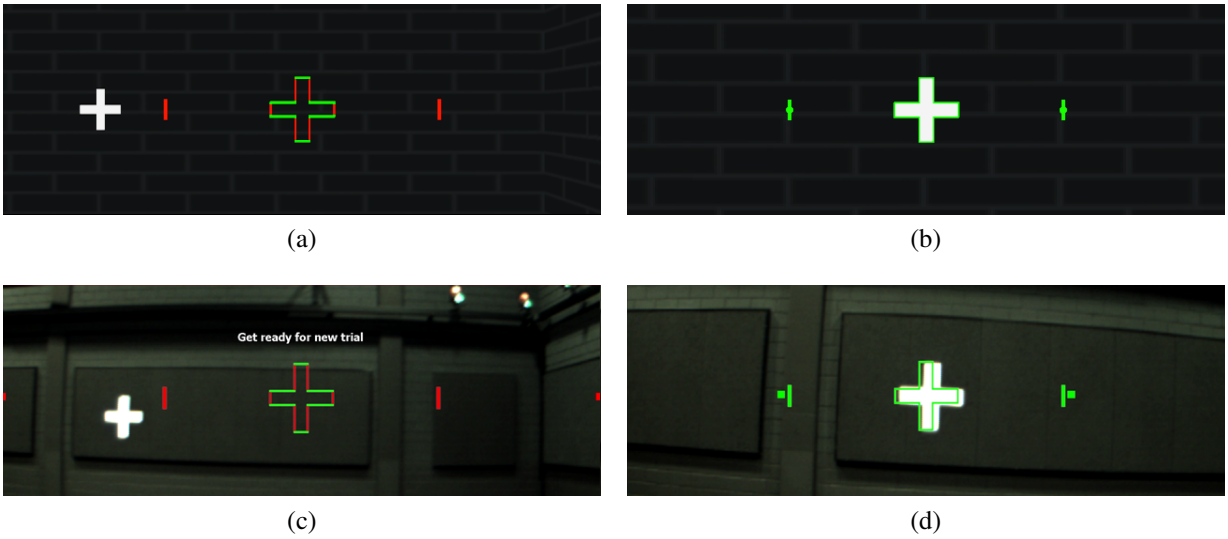

(a) (b) (c) (d)

Fig. 7: Camera views relative the the starting (Fig. (a)) and goal (Fig. (b)) locations in the simulated environment. Figures (c) and (d) show the same views from the real quadcopter camera

moved along a horizontal line passing through the image center. The horizontal position of the right dot was proportional to the relative depth between the quadcopter and the target location, so that the smaller the depth, the closer the dot to the image center. The left dot was moved symmetrically from the left side of the image. Two small vertical bars indicated the required location of the two dots when at P_1 and were used by the subjects as a direct measure of the depth error from the target location. Finally, all these artificial cues had a red color when outside of the box B, and a green color when inside B. This color cue was useful for judging when the quadcopter entered the target box.

As for the vestibular feedback, 3 different conditions were tested

1. normal motion (*grav*);
2. artificial motion (*aff*);
3. no motion (*vis*).

In the condition *grav*, the CyberMotion simulator was actuated so as to reproduce the forward and lateral components of gravity in the body frame B as a consequence of the quadcopter rotation in the world frame. In this way, the subjects could use this motion cue to infer the quadcopter orientation (and thus its world acceleration) besides what they could visually perceive from the camera images. After several pilot trials, this rotation was artificially amplified by a factor 3 to enhance the effect of the pitch/roll commands typically needed to control the quadcopter motion. Indeed, because of the limited space in the tracking hall and the fine adjustments needed in the neighborhood of P_1, the quadcopter is almost never tilted more than 6 deg, thus resulting in very small components of the gravity acceleration in body frame. Figure 10 shows a typical profile of the angles (ϕ, θ) during one trial.

In condition *aff*, we used the CyberMotion simulator to reproduce an artificial acceleration proportional to the Cartesian vector from the current position to the target location P_1 scaled by a factor 1.5 $1/s^2$ and limited to a maximum of 3 $\mathrm{m/s^2}$. As opposite to the previous case, this motion cue was meant to inform the subjects on where to steer in order to complete the task rather than on their current motion status.

Finally, in the last condition *vis*, the subjects fulfilled the task by relying on the sole visual feedback.

Experimental procedure

The aforementioned 3 feedback conditions were tested in the two scenarios of controlling both the real quadcopter and its software simulation model. Every condition was tested in blocks of $n_T = 3$ consecutive trials, and $n_B = 3$ of these blocks in a row (one for each condition) were run before giving the subjects a break. The order of the n_B blocks was randomly permuted. This procedure was repeated 3 times for a total of $3 \times n_T \times n_B = 27$ single trials when controlling the real quadcopter, and likewise $3 \times n_T \times n_B = 27$ single trials when controlling the simulated quadcopter. Therefore, every subject was exposed to a total of 54 trials. Every trial was limited to a maximum of 4 minutes.

Before each new block was started, the test subjects were told the motion condition they were exposed to in the following n_T trials. We also allowed the test subjects some rest from trial to trial.

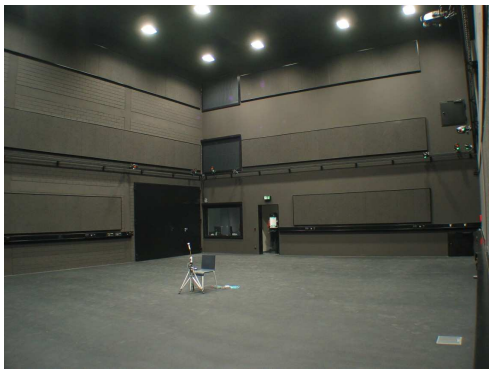

(a)

(b)

Fig. 8: Details of the tracking hall

We had 16 naive test subjects, 5 of them female and 11 male. All of them were between the age of 22 and 32, on average 26.2. Four of these 16 subjects were not able to do the task at all, 3 of them female and 1 male. The test subjects were instructed to fly to the target position and to hover there for 3 seconds. They were not explicitly instructed on effective strategies to control the quadcopter motion, but were informed that their available control inputs (roll and pitch) are directly responsible for the forward and lateral accelerations of the quadcopter, and that the yaw and height were automatically regulated by the onboard controller. Furthermore, they were also informed about the presence of a delay of about 300 ms between their command actions and the resulting visual/vestibular feedbacks[2].

All the subjects performed 2 test trials before actually starting the experiment for getting them acquainted with the system and the instructions. On average every subject needed about 2 hours to complete all 27 trials with the real quadcopter, and about 1 hour for the 27 trials with the simulated quadcopter.

[2]This delay is mainly due to latencies in the network link between the QFC and the Motion Simulator Control PC (250 ms), and to an additional delay of 40 ms between the Motion Simulator Control PC and the actuation system of our motion simulator (see Fig. 4).

Fig. 9: The remote control used for the experiments

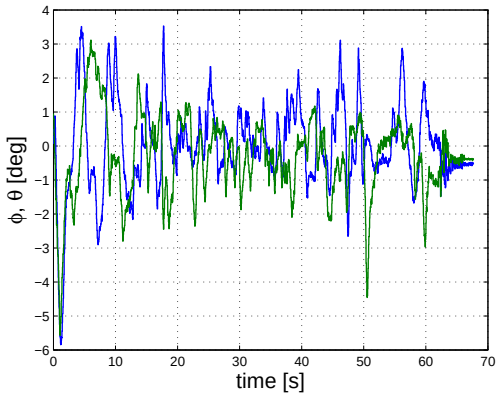

Fig. 10: Behavior of the UAV angles (ϕ, θ) over time during one trial

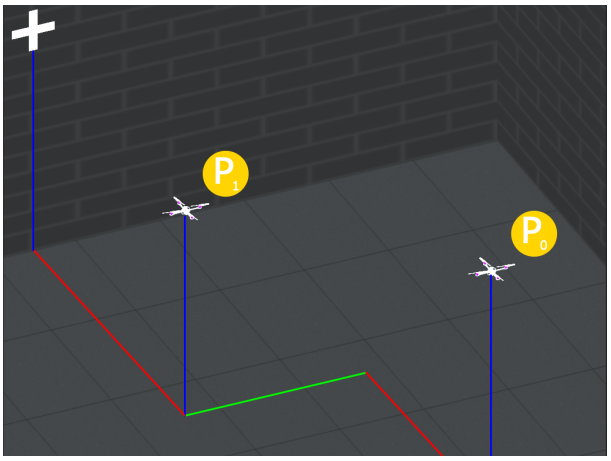

Fig. 11: Overview of the starting position P_0 and the target position P_1 in the simulated tracking lab

Results

The performance of the subjects in remotely piloting the UAV was evaluated by considering the average total time needed to complete the task and the average control effort (roll and pitch commands) sent to the UAV during the trials. The differences in performance were analyzed by resorting to the standard statistical tools (mixed model ANOVA (Ref. 26)).

	grav	*aff*	*vis*	*overall*
simulation	60.384	66.65	44.75	56.94
real	67.67	71.51	66.68	68.56

Table 1: Average completion time over all trials and subjects in the different conditions

	grav	*aff*	*vis*	*overall*
simulation	0.08498	0.1093	0.1096	0.1013
real	0.1306	0.1474	0.1509	0.1428

Table 2: Average control effort over all trials and subjects in the different conditions

Completion time

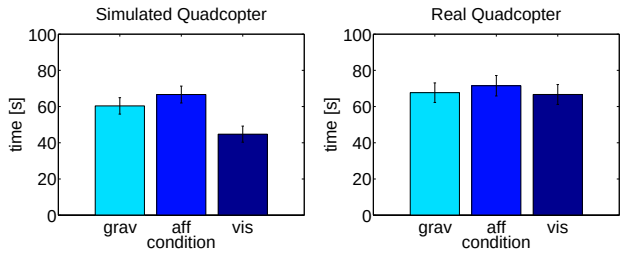

(a) (b)

Fig. 12: Overall average time per condition with simulated quadcopter (a) and real quadcopter (b)

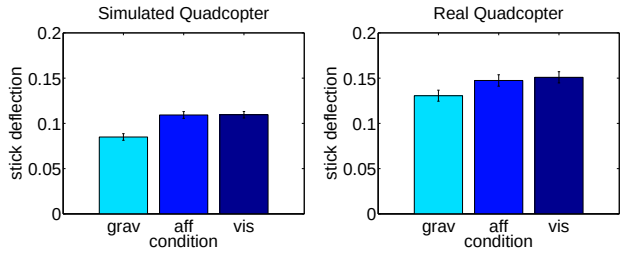

(a) (b)

Fig. 13: Overall control effort per condition with simulated quadcopter (a) and real quadcopter (b)

All the trials in which the test subjects exceeded the time limit were removed before the data was evaluated. Table 1 and Fig. 12(a–b) report the average time over all trials and subjects for the different conditions. In all conditions the subjects needed in average more time to complete the task when piloting the real quadcopter compared to the simulated quadcopter. This difference in performance was found significant in the *vis* condition ($F(1,193) = 11.5$, $p = .001$, about 22 s), and not significant in the other two conditions (*grav*: $F(1,192) = 1.1$, $p = .297$, *aff*: $F(1,179) = 0.38$, $p = .538$).

Within the trials with the simulated quadcopter, we also found a significant difference between the three motion conditions ($F(2,296) = 6.216$, $p = 0.0023$), with the subjects performing best in the *vis* condition (Fig. 12(a)). This was not the case when piloting the real quadcopter, where the differences were found not significant over all the subjects ($F(2,268) = 0.2091$, $p = 0.8114$). However, if we look at the individual performance over all trials in the real quadcopter case (Fig. 14), only subject 12 showed significant differences between the conditions ($F(2,18) = 4.532$, $p = 0.025$) and was best with the *grav* motion feedback.

Control effort

As a measure of the control effort spent by the subjects, we considered the quantity $\sqrt{s_\phi^2(t) + s_\theta^2(t)}$ averaged over the whole trial. Table 2 and Fig. 13 show the results over all trials and test subjects. As opposite to the previous case, we found a significant difference among the three conditions both within the simulated quadcopter trials ($F(2,298) = 14.83, p < 0.001$, Fig. 13(a)), and within the real quadcopter trials ($F(2,270) = 3.124, p = 0.04557$, Fig. 13(b)). In both cases, the subjects spent significantly less control effort in the *grav* condition, followed by the *aff* condition and then by the *vis* condition.

Discussion

The data relative to the completion time showed a large difference when piloting the simulated and real quadcopter in the *vis* condition. We believe that this is due to the different quality of visual feedback in these two cases. In simulation, the camera images run smoothly at 60 fps without any frame drop, while in the real case the images were refreshed at a rate between 20 and 25 fps, and suffered from several frame drops during the trials because of network congestion. These data losses negatively affected the performance because of the fine adjustments required in the chosen task, and visual feedback played a predominant role in judging the relative position w.r.t. the target. It should be noted, however, that in real scenarios it is unlikely to have a perfect visual feedback as in the simulation case, especially if the distances involved in the teleoperation task are much larger than the ones in our experiments (about 10 m). In this case, additional cues, such as our motion cues, could compensate for the missing visual information, but our results in flying the real quadcopter were not conclusive in this sense.

On the other hand, by analyzing the control effort spent by the subjects, we clearly found that the amount of input commands was correlated with the tested conditions. In particular, in the *grav* condition the subjects had more 'gentle' control actions compared to the *aff* and *vis* conditions. This result can be explained by the fact that, in the *grav* condition, the subjects could directly feel the UAV motion and thus were more careful in applying strong or erratic commands as if they were piloting from onboard. This

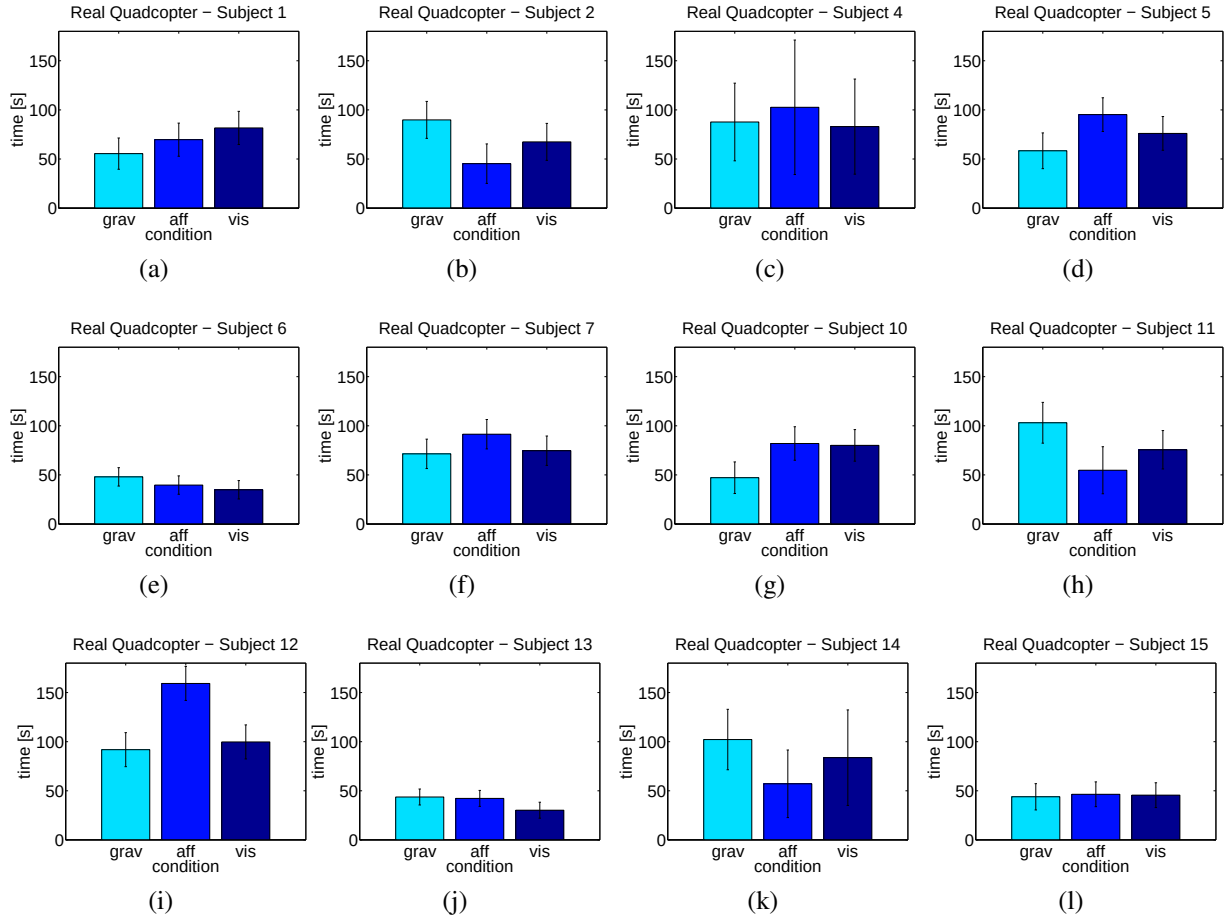

Fig. 14: Average time per condition for each of the 12 test subjects, real quadcopter

phenomenon, denoted as *shared fate* in (Ref. 15), is a consequence of the improved situational awareness of the test subjects in the *grav* condition. Often pilots report that, by feeling the accelerations they are exposed to, they can become aware of dangerous loads and stresses in the aircraft structure and avoid too risky maneuvers. Of course, lack of this information in a remote control scenario may be dangerous for the UAV safety and ultimately lead to unnecessary losses that could be avoided by providing the correct motion cues to the ground operator.

As a final remark, also when looking at the control effort, the *aff* condition was not found significantly different than the *vis* condition ($F(1, 199) = 0.002$, $p = 0.966$ in the simulated case, and $F(1, 177) = .147$, $p = 0.702$ in the real case). A possible explanation is that taking advantage of this kind of feedback requires too much cognitive workload or training, and thus the subjects did only rely on the visual feedback. This was also orally reported by the test subjects after completing their trials.

Conclusions

The improvement of the situational awareness for ground operators of UAVs is an essential component in making the whole architecture less prone to human errors because of misinterpretation of the UAV status. In this sense, our work represents a step towards the ideal goal of obtaining a perfect telepresence system in remote control tasks. Our contribution is twofold: we presented the implementation of an experimental setup for testing our visual-vestibular feedback concept, and ran a systematic evaluation on how such a system could improve the human operator performance. We believe that the results found in our experimental tests indicate a promising direction for the proposed visual-vestibular teleoperation method.

Of course, many improvements are still needed and will be addressed in future developments. For instance, we will minimize the (unavoidable) sources of delay in the system by optimizing the communication links between the various components, and will design and test different tasks besides the simple hovering maneuvers presented in this work. We are also planning to test this concept with other types of UAVs such as medium or full scale rotorcraft or fixed-wing vehicles, as well as switching to outdoor testing and directly

use the UAV onboard measurements of accelerations and GPS positions as sources of motion data.

Acknowledgments

This research was supported by the Max Planck Society and by the WCU (World Class University) program through the National Research Foundation of Korea funded by the Ministry of Education, Science and Technology (R31-2008-000-10008-0). We are grateful to Dr. Harald Teufel, Karl Beykirch and Michael Kerger for their intensive technical support, and to Dr. Tobias Meilinger for his help in designing the experimental conditions and in analyzing the results.

References

[1]Unmanned Flight Control: Multiple UAVs for Coverage and Surveillance , Vol. 16, (2), IEEE Robotics and Automation Magazine, 2009.

[2]Murphy, R. R. and Burke, J. L., "From Remote Tools to Shared Roles," *IEEE Robotics & Automation Magazine*, Vol. 15, (4), 2008, pp. 39–49.

[3]Drury, J., Scholtz, J., and Yanco, H. A., "Awareness in Human-Robot Interactions," Proc. IEEE Int. Conf. on Systems, Man and Cybernetics, Vol. 1, 2003.

[4]Parush, A., "Human Errors in UAV Takeoff and Landing: Theoretical Account and Practical Implications," *Advances in Human Performance and Cognitive Engineering Research*, Chap. 7, Emerald, 2006, pp. 91–103.

[5]Airforce Technology, "http://www.airforce-technology.com/projects/predator," .

[6]Wikipedia, "http://en.wikipedia.org/wiki/MQ-1_Predator," .

[7]Mittelstaedt, H., "A new solution to the problem of the subjective vertical," *Naturwissenschaften*, Vol. 70, (6), 1983, pp. 272–281.

[8]Angelaki, D. E., McHenry, M. Q., Dickman, J. D., Newlands, S. D., and Hess, B. J. M., "Computation of Inertial Motion: Neural Strategies to Resolve Ambiguous Otolith Information," *The Journal of Neuroscience*, Vol. 19, (1), 1999, pp. 316–327.

[9]Merfeld, D. M., Zupan, L., and Peterka, R. J., "Humans use internal models to estimate gravity and linear acceleration," *Nature*, Vol. 398, 1999, pp. 615–618.

[10]Mittelstaedt, M. L. and Mittelstaedt, H., "Idiothetic navigation in humans : estimation of path length," *Experimental brain research*, Vol. 139, (3), 2001, pp. 318–332.

[11]Angelaki, D. E., Shaikh, A. G., Green, A. M., and Dickman, J. D., "Neurons compute internal models of the physical laws of motion," *Nature*, Vol. 430, 2004, pp. 560–564.

[12]MacNeilage, P. R., Banks, M. S., Berger, D. R., and Bülthoff, H. H., "A Bayesian model of the disambiguation of gravitoinertial force by visual cues," *Experimental Brain Research*, Vol. 170, (2), 2007, pp. 263–290.

[13]Maza, M., Baselga, S., , and Ortiz, J., *Climbing and Walking Robots*, Springer Berlin Heidelberg, 2006, Chapter Vehicle Teleoperation with a Multisensory Driving Interface, pp. 437–445.

[14]Ortiz, J., Tapia, C., Rossi, L., Fontaine, J.-G., and Maza, M., "Description and tests of a multisensorial driving interface for vehicle teleoperation," *Proc. of the IEEE 11th Int. Conference on Intelligent Transportation Systems*, 2008, pp. 616–621.

[15]Hing, J. T. and Oh, P. Y., "Development of an Unmanned Aerial Vehicle Piloting System with Integrated Motion Cueing for Training and Pilot Evaluation," *Journal of Intelligent and Robotic Systems*, Vol. 54, (1–3), 2009, pp. 3–19.

[16]VICON Motion Capture, "http://www.vicon.com/," .

[17]Robocoaster, "www.robocoaster.com," .

[18]Teufel, H., Nusseck, H.-G., Beykirch, K. A., Butler, J. S., Kerger, M., and Bülthoff, H. H., "MPI Motion Simulator: Development and Analysis of a Novel Motion Simulator," Proc. AIAA Modeling and Simulation Technologies Conference, 2007.

[19]Beykirch, K., Nieuwenhuizen, F. M., Teufel, H., Nusseck, H.-G., and Bülthoff, H. H., "A Roll-Lateral Helicopter Side-Step Maneuver on the MPI Motion Simulator," Proc. AHS 64th Annual Forum, 2008.

[20]Nusseck, H.-G., Teufel, H. J., Nieuwenhuizen, F. M., and Bülthoff, H. H., "Learning System Dynamics: Transfer of Training in a Helicopter Hover Simulator," Proc. AIAA Modeling and Simulation Technologies Conference, 2008.

[21]Nieuwenhuizen, F. M., Zaal, P. M., Teufel, H. J., Mulder, M., and Bülthoff, H. H., "The Effect of Simulator Motion on Pilot Control Behaviour for Agile and Inert Helicopter Dynamics," submitted to the AIAA Modeling and Simulation Technologies Conference, 2009.

[22]Robuffo Giordano, P., Masone, C., Tesch, J., Breidt, M., Pollini, L., and Bülthoff, H. H., "A Novel Framework for Closed-Loop Robotic Motion Simulation - Part I: Inverse Kinematics Design," *to appear in the 2010 IEEE Int. Conf. on Robotics and Automation*, 2010.

[23]Robuffo Giordano, P., Masone, C., Tesch, J., Breidt, M., Pollini, L., and Bülthoff, H. H., "A Novel Framework for Closed-Loop Robotic Motion Simulation - Part II: Motion Cueing Design and Experimental Validation," *to appear in the 2010 IEEE Int. Conf. on Robotics and Automation*, 2010.

[24]HiSystems GmbH, “http://www.mikrokopter.de/,” .

[25]Bouabdallah, S. and Siegwart, R., *Advances in Unmanned Aerial Vehicles*, Springer Press, 2007, Chapter Design and Control of a Miniature Quadrotor, pp. 171–210.

[26]McLean, R. A., Sanders, W. L., and Stroup, W. W., “A Unified Approach to Mixed Linear Models,” *The American Statistician*, Vol. 45, (1), 1991, pp. 54–64.